Article

Investigation on Slot–Pole Combinations of a PM Vernier Motor with Fractional-Slot Concentrated Winding Configurations

Byungtaek Kim

Department of Electrical Engineering, Kunsan National University, Gunsan-si 54150, Korea;
btkim@kunsan.ac.kr; Tel.: +82-063-469-4744

Abstract: This paper presents a new method to find available slot–pole combination of a permanent magnet (PM) vernier motor with fractional-slot concentrated winding (FSCW) configurations instead of the conventional design rule. To this aim, for a common structure of PM vernier machines with FSCW, the air gap flux densities including modulation flux due to vernier effects are investigated from the magnetic view points and then a general condition to effectively use the modulation flux is derived. Under the obtained condition, the specific design condition for slot–pole combinations are established for the most popular FSCW configurations with the coil spans of $\pm 2\pi/3$. Using the established condition, all available vernier structures including those which could not be found by the previous rule are obtained, and the back-electromotive force (EMF) of each structure is analytically estimated to check the vernier effects. During these procedures, it is also revealed that some of general FSCW-PM motors possess vernier effects and thus can be classified into vernier motors. To verify the proposed ideas, the characteristics of back EMF are analyzed through finite element (FE)-simulations for various models, and compared with their analytical calculation results. Finally, the characteristics of torque regarding to slot–pole combinations of the vernier motors are discussed.

Keywords: fractional-slot concentrated winding; modulation flux; permanent magnet; vernier motor

1. Introduction

The vernier PM motor is being recently considered a strong candidate able to meet the needs for higher power density, especially in low-speed electro-mechanical systems such as electric vehicles and wind power generators. The motor uniquely makes use of a modulation flux through the reaction between the slot harmonic of air gap permeance and the magneto-motive force (MMF) of rotor PM, the so called 'vernier effect', as well as a common flux due to PM, consequently resulting in higher back EMF and thus higher power. In order to bring about the modulation flux, the well-known rule $p_m - Q_s = -p_w$ is commonly used where p_m, Q_s, and p_w are the numbers of magnet pole pairs, stator slots (or called the flux modulation pole), and winding pole pairs, respectively [1–4]. This rule can be readily applied to the distributed-winding machines, however, these windings generally employ lengthy end-turns with higher copper losses, and thus fractional-slot concentrated windings (FSCW) are preferred [5].

On the other hand, there can be an uncertainty when one applies the previous rule to the machine with FSCWs, because the winding pole-pairs p_w of FSCW configurations can be ambiguous as follows. In a PM machine with traditional distributed windings, p_w is very apparent and equal to the magnet pole-pairs p_m, which implies that the power conversion takes place with the interaction between the both magnetic fields from stator windings and PM with same pole pairs. Meanwhile, as the simplest examples, two popular types of FSCW-PM machines can be considered, as follows. It is assumed that both machines have the identical stator with three slots, but one has two PM poles and

the other has four PM poles. According to the field-interaction principle, it is reasonable to think that the one with two PM pole has two winding poles, and the other with four PM poles has four winding poles, demonstrating the identical stators can have different winding poles. However, in quite many studies, the FSCW-PM vernier machines built upon the previous rule have been proposed under the assumption that three slots of a FSCW machine make up one winding pole pair [6–10]. This assumption is obviously useful as well as convenient to design the vernier machine, but there is still uncertainty whether the conventional rule under the assumption provides every available slot–pole combinations for the vernier machine.

In this study, to avoid this ambiguity associated with winding pole pairs and to find every available vernier structure with FSCW configurations, firstly, both the useful air gap fluxes are expressed for a generalized PM vernier structure, and then the induced voltage of a single conductor due to the both fluxes are investigated from an electro-magnetic view point. The single conductor voltage equation leads to the necessary condition to utilize the modulation flux and the common PM flux as well. By coupling the condition with a given slot angle for three phase FSCWs, the criterion for slot–pole combination of the vernier machines can be specified. As a useful example, with very popular slot angle $\pm 2\pi/3$ of FSCWs, the criterion for the combination is presented. Using the criterion, the available combinations for vernier machines are obtained and the results are compared with those obtained from the previous rules, which reveals that the proposed method helps find many more available slot–pole combinations for the FSCW vernier PM machine. In addition, from the results, it is also revealed that some of the conventional FSCW-PM machines can be classified into vernier machines. To investigate the individual effects of modulation flux and conventional PM flux on the back EMF, the well-organized back EMF equations are provided the back EMF of the obtained models are analytically calculated. Finally, FE simulations are carried out for various models to check the proposed, and the results are compared with the analytical calculation results.

2. Air Gap Flux of a FSCW-PM Vernier Machine

2.1. General Structure of a SPM Vernier Machine with FSCWs

Figure 1 shows a surface PM (SPM) vernier machine with p_m magnet pole pairs in which three adjacent stator slots provide the area for the three-phase slot-concentrated windings. To generalize the structure of vernier machine, it is assumed that each stator tooth has n_{aux} auxiliary poles (teeth), and thus the total flux modulation poles Q_{fmp} is equal to $n_{aux}Q_s$ where Q_s is again the number of stator slots.
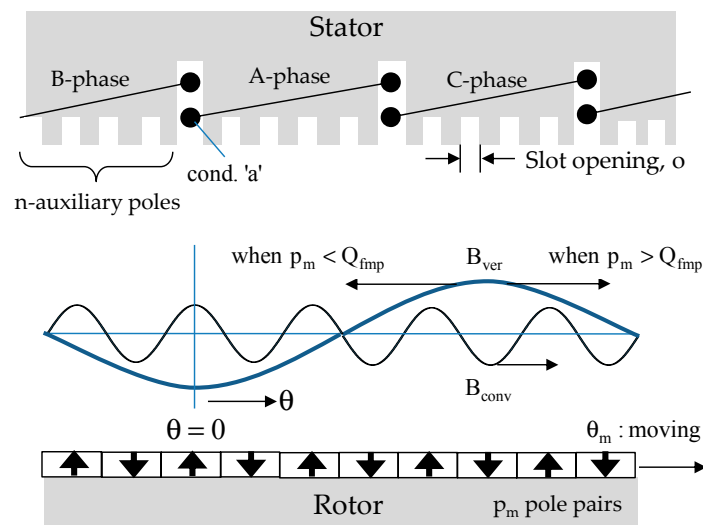
Figure 1. Conceptual structure of a FSCW-PM vernier motor.

2.2. Air Gap Flux Density Equation

In the SPM structure of Figure 1, the magneto-motive force(MMF) of rotor PMs can be approximately represented by (1) with the fundamental component of the MMF wave $F_{1.m}$, where θ and θ_m stand for the angular position in air gap and the angular movement of rotor, respectively.

$$F_{mag} \approx F_{1.m} \cos\{p_m(\theta - \theta_m)\} \tag{1}$$

In (1), $F_{1.m}$ is expressed as (2) where g_a is the air gap length, g_m is the magnet thickness, B_r is the remanence flux density of PM, μ_{rec} and μ_0 are the recoil permeability of PM and the permeability of vacuum, respectively.

$$F_{m.1} = \frac{4}{\pi} \frac{B_r g_m}{\mu_{rec} \mu_0} \tag{2}$$

Next, the air gap is uneven due to the stator teeth and the auxiliary poles. If the reference position of $\theta = 0$ is at the center of the slot and all slot-open widths are same as shown in Figure 1, the specific permeance of the air gap is provided as:

$$\Lambda_g \approx P_0 - P_1 \cos\left(Q_{fmp}\theta\right), \tag{3}$$

where the coefficient P_0 and P_1 reflect the average and the first harmonic values of the permeance, respectively, and they can be expressed in classical form using the conformal mapping method [11]. The resulting values are given as (4) and (5) in terms of geometries of the machine where g_{m+a} is the effective gap length considering magnet thickness, given by $g_m/\mu_{rec} + g_a$. The factor c_0 is the ratio of the slot open o to the slot pitch $2\pi r_g/Q_{fmp}$. Finally, β in (4) and (5) is a non-linear coefficient, given as (6).

$$P_0 = \frac{\mu_0}{g_{m+a}} (1 - 1.6\beta c_0) \tag{4}$$

$$P_1 = \frac{\mu_0}{g_{m+a}} \frac{2\beta}{\pi} \left(\frac{0.39}{0.39 - c_0{}^2}\right) \sin(1.6\pi c_0) \tag{5}$$

$$\beta = \frac{1}{2} - \frac{1}{\sqrt{4 + \left(\frac{o}{g_{m+a}}\right)^2}} \tag{6}$$

By multiplying the PM's MMF of (1) and the specific air gap permeance of (3), the air gap flux wave is obtained as (7), where another wave with $p_m + Q_{fmp}$ pole pairs whose speed is $p_m/(p_m + Q_{fmp})\cdot\omega_m$ has been ignored since its speed is quite low and thus develops negligible back EMF [2].

$$
\begin{aligned}
B_g &\approx F_{1.m}P_0 \cos\{P_m(\theta - \theta_m)\} - \frac{F_{1.m}P_1}{2} \cos\left\{(P_m - Q_{FmP})\left(\theta - \frac{P_m}{P_m - Q_{fmP}}\theta_m\right)\right\} \\
&= B_{conv} + B_{ver}
\end{aligned}
\tag{7}
$$

Equation (7) clearly shows both fluxes, B_{conv} with p_m pole pairs and B_{ver} with $p_{ver}(= |p_m - Q_{fmp}|)$ pole pairs, and their mechanical angular speeds are $\omega_m(= d\theta_m/dt)$ and $p_m/(p_m - Q_{fmp})\cdot\omega_m$, respectively. In addition, it should be noted that the rotational direction of B_{ver} depends on the sign of $p_m - Q_{fmp}$. In other words, the traveling directions of both flux are same when $p_m - Q_{fmp} > 0$ and opposite when $p_m - Q_{fmp} < 0$ as depicted in Figure 1. Despite the speed difference, the time derivatives of both fluxes at any position have the same frequency. For example, B_g at $\theta = 0$ is given by (8), showing the both same frequency of $p_m\omega_m$. In particular, both waves are passing with their (+) and (−) maximum values at the instance of $\theta_m = 0$.

$$
\begin{aligned}
B_g(\theta = 0) &\approx F_{1.m}P_0 \cos(P_m\theta_m) - \frac{F_{1.m}P_1}{2} \cos(P_m\theta_m) \\
&= \hat{B}_{conv} \cos(P_m\theta_m) - \hat{B}_{ver} \cos(P_m\theta_m)
\end{aligned}
\tag{8}
$$

3. Slot–Pole Combinations of a PM Vernier Machine with Concentrated Windings

3.1. Necessary Condition for Vernier Effects Utilization

As mentioned with (7), there are both flux waves in the air gap. Thus, so as to obtain higher back EMF, both back EMFs from B_{conv} and B_{ver} need to be additive. To find the condition for this operation, it is convenient to check the induced voltage of conductor 'a' at the position of $\theta = 0$ and at the instance of $\theta_m = 0$, since the both fluxes have their (+) and (−) peak values ($\hat{B}_{conv}$ and $-\hat{B}_{ver}$) as explained already with (8). By using the principle that the induced voltage of a conductor e = vB, where v is the relative speed of B to the conductor. Since the relative speeds of the waves are given as $v_{conv} = -r_g\omega_m$ and $v_{ver} = -r_g\,p_m/(p_m - Q_{fmp})\cdot\omega_m$, the instantaneous voltage e_a in the conductor with unit length is given by (9).

$$
\begin{aligned}
e_a &= -v_{conv}\hat{B}_{conv} - v_{ver}\hat{B}_{verp} \\
&= -r_g\omega_m\big(\hat{B}_{conv} + G_r\hat{B}_{vre}\big)
\end{aligned}
\tag{9}
$$

where r_g is the air gap radius and $G_r = -p_m/(p_m - Q_{fmp})$ which is the so-called gear ratio [9] which contributes higher back EMF of vernier PM machines than conventional PM machines.

From (9), it is clear that both EMFs are additive and the magnitude of e_a is maximized when $G_r > 0$ alternatively, $Q_{fmp} - p_m > 0$. Therefore, the relation $Q_{fmp} - p_m > 0$ is the necessary condition to effectively utilize the back EMF due to B_{ver}, which also indicates both waves need to move in opposite direction each other. Meanwhile, this condition is obtained from only one conductor 'a' in Figure 1, so it is also necessary to check whether the EMFs of other conductors still additive under the condition. It can be proved by investigating the slot angle which are the angles between both adjacent slots for B_{conv} and B_{ver}. Figure 2 demonstrates the slot angles α_{conv} and α_{ver} for the both flux waves. The angle α_{conv} for B_{conv} with p_m poles can be easily represented as (10). On the other hand, the angle α_{ver} for B_{ver} with $p_{ver} = |p_m - Q_{fmp}|$ should be obtained with consideration of its opposite traveling direction to B_{conv}, and can finally be obtained as (11) by using relation $Q_{fmp} = n_{aux}Q_s$.

$$
\alpha_{conv} = \frac{2\pi}{Q_s}p_m
\tag{10}
$$

$$
\alpha_{ver} = -\frac{2\pi}{Q_s}p_{ver} = \frac{2\pi}{Q_s}(p_m - n_{aux}Q_s) = \frac{2\pi}{Q_s}p_m
\tag{11}
$$

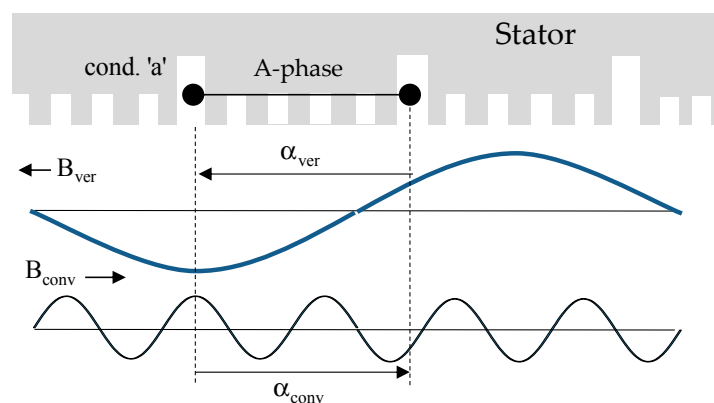**Figure 2.** Slot angles for both flux waves.

From (10) and (11), it is clear the both angles α_{conv} and α_{ver} are always same under the necessary condition $Q_{fmp} - p_m > 0$ and thus the back EMFs are additive for every conductor. It reveals another interesting fact that most of FSCW-PM machines considered as general PM motors can be classified as vernier machines. For example, the machines with the very popular ratios of three slots/two magnet poles and three slots/four magnet poles are commonly considered as general FSCW-PM machines.

Therefore, in most previous references or textbooks, the characteristics of these machines are explained with only the conventional PM flux (which is B_{conv} in this study) without considering the modulation flux, consequently there was no difference in the fundamental magnitudes of the back EMFs of both machines [12–14]. However, the slot pole combinations of the machines satisfy the necessary condition $Q_{fmp} - p_m > 0$ where Q_{fmp} are both 3 because of $n_{aux} = 1$, and p_m are 1 and 2, respectively, which means they possess the modulation flux as well as conventional PM flux. Thus, they can be classified as vernier machines in a special case of *n* = 1, and it is necessary to consider the modulation flux effects on the back EMF of the machines which will be investigated in the chapter IV of this paper.

3.2. Derivation of Design Criteria for Various Auxiliary Poles

Based on the obtained necessary condition, the complete criteria for the slot–pole combinations of FSCW-PM vernier machines are proposed. To this end, the slot angle $\alpha_{conv}(=\alpha_{ver})$ for the flux B_{conv} is assumed to be $2\pi/3$ or $4\pi/3(=-2\pi/3)$ which are the most popular winding configurations since it has one slot coil pitch. With these angles, the minimum number of the slots for a complete machine is three. If the criteria are developed for three slots ($Q_s = 3$), they are easily expanded to the machines whose slot number is q multiple of three. For the structure with n_{aux} auxiliary poles in Figure 1, the angle α_{ver} of (10) can be given as (12) by using $Q_s = Q_{fmp}/n$.

$$\alpha_{ver}(=\alpha_{conv}) = 2n\pi\frac{P_m}{Q_{fmp}} = \pm\frac{2\pi}{3} + 2k\pi, \tag{12}$$

where n = 1, 2, 3, ... , and k = 0, ±1, ±2, ±3, ...

By solving (12) for p_m, the complete criteria for the combinations of the FSCW vernier machines with the slot angle of $\pm 2\pi/3$ are obtained as (13). It should be mentioned that the obtained criteria can be used without considering the winding pole pair p_w in conventional rule, $p_m - Q_{fmp} = -p_w$.

$$p_m = \pm\frac{1+3k}{3n_{aux}}Q_{fmp} = \pm(1+3k) \text{ for } Q_{fmp} - p_m = 3n_{aux} - p_m > 0 \tag{13}$$

For the various auxiliary poles of n_{aux} = 1~3, every available number of p_m for a FSCW-PM vernier machine with three slots ($Q_s = 3$) are acquired by using (13), resulting in 12 combinations in total. They are listed in Table 1 with additional parameters such as p_{ver} and G_r. These combinations can be compared with the combinations from previous rules. If the previous rule $p_m = Q_{fmp} - p_w = n_{aux}Q_s - p_w$ is used with the assumption of $p_w = 1$ for three slots ($Q_s = 3$), only three combinations can be obtained for same n_{aux} = 1~3, which are p_m = 2, 5, 8, respectively. It means the proposed method widens the range of choice of slot–pole combinations, and helps to check the existence of the vernier effects in any PM machine.

Table 1. Proposed p_m (PM pairs) for a three-slot FSCW vernier motor with various n_{aux}.

Aux. Pole Numbers n_{aux}	k	PM Pairs p_m	$p_{ver} = Q_{fmp} - p_m$	$G_r = p_m/p_{ver}$
1	0	1	2	1/2
	−1	2	1	2
2	0	1	5	1/5
	−1	2	4	1/2
	1	4	2	2
	−2	5	1	5
3	0	1	8	1/8
	−1	2	7	2/7
	1	4	5	4/5
	−2	5	4	5/4
	2	7	2	7/2
	−3	8	1	8

Besides, as expected in the last section, the models with $p_m = 1$ and 2 are included for $n_{aux} = 1$ in Table 1 as vernier structures. In fact, there is a reason why they have not been considered as vernier machines so far. It is that the vernier effects in the both models are not significant, which can be explained as follows. Since P_0 is certainly larger than P_1 in (3), it is apparent that $\hat{B}_{conv}$ is quite greater than $\hat{B}_{ver}$ from (7), and thus the significance of vernier effects in the total back EMF depends on the gear ratio G_r in (8). In this respect, the values of G_r of the both models in the Table 1 are relatively small at 1/2 and 2 respectively, and thus $\hat{B}_{conv}$ is still dominant rather than $G_r\hat{B}_{ver}$ in (8). With the same reason, the models with $p_m = 5$ for $n_{aux} = 2$ and $p_m = 8$ for $n_{aux} = 3$ whose G_r values are 5 and 8 respectively are expected to produce quite higher back EMF comparing to the model with $p_m = 1$ for $n = 1$.

4. Analytical Calculation of Vernier Effects and Verifications through FE-Simulations

To check vernier effects on the back EMF of the obtained models, the back EMF of each models in Table 1 are analytically calculated with analytical method, and then the analytical calculation results are compared with FE-simulation results. To this end, firstly, the geometries of the analysis models are assumed to have common specifications in Table 2. Every model has the same air gap radius r_g, the air gap length g_a, the same PM thickness g_m and the same stack length l_{stk}, which keeps the magnetic loading same for each models. The ferrite magnet is assumed for the PM whose B_r is 0.4T. The slot open ratio c_0 of, in particular, is set to 0.5 because the vernier effects tend to be maximized at the value according to previous studies [2,3]. To keep the same electric loading, every model has the same number of series-turns/phase N_{ph}, and the same current is applied. With these conditions, the back EMF of each model is finally calculated at 500rpm of rotational speed.

Table 2. Common specifications of the analysis models.

Quantity	Value	Quantity	Value
Air gap radius r_g	25 mm	PM residual flux density B_r	0.4T (ferrite)
Air gap length g_a	0.5 mm	Magnet thickness g_m	2 mm
Stack length l_{stk}	100 mm	Total series number of turns/phase N_{ph}	220
Rotational speed	500 rpm	Armature phase current	2A

4.1. Analytical Calculations of Back EMF using a Single Conductor Voltage

In order to calculate the back EMF, the coefficients P_0, P_1, and β for the given geometries are firstly investigated by using (4) and (5) with the number of auxiliary poles, n_{aux} as shown in Figure 3, where it should be noted that P_0, P_1, and β are independent with the number of magnet pole pairs, p_m. It illustrates as n_{aux} increases, the coefficient β decreases because the slot opening o decreases with n_{aux} while the gap is kept constant as represented in (6). From (4) and (5), it is natural that the tendencies of specific permeance, P_0 and P_1, in Figure 3b are opposite each other. With the obtained P_0 and P_1, the both peak flux densities $\hat{B}_{conv}$ and $\hat{B}_{ver}$ are calculated by using (7) for the combinations in Table 1. Using (8), the induced voltages $\hat{e}_{a.conv}$ and $\hat{e}_{a.ver}$ due to both flux densities $\hat{e}_{conv}$ and $\hat{B}_{ver}$, and their sum, that is, the peak induced voltage $\hat{e}_a$ of the conductor 'a' is calculated at 500 rpm in which the factor G_r in Table 1 is used.
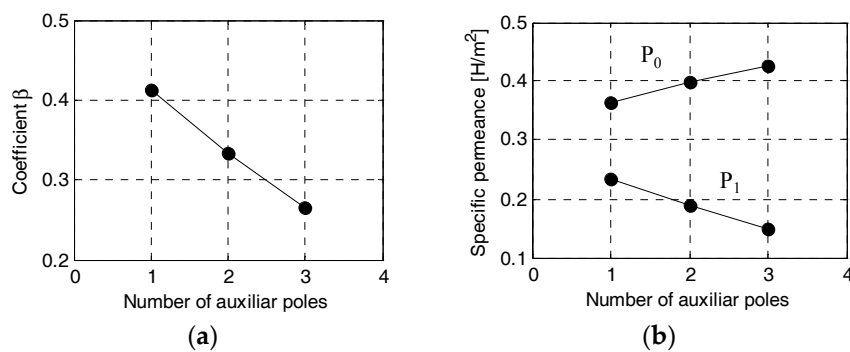
Figure 3. Variation of β and specific permeance with the auxiliary poles. (**a**) β; (**b**) Specific permeance P_0 and P_1.

The calculated results through the procedure explained above are listed in Table 3. In case of $n_{aux} = 1$, two models with $p_m = 1$ and 2 have the same voltage from general PM flux. On the other hand, their voltages due to vernier effects are quite different, and thus the model with $p_m = 2$ has higher back EMF than the one with $p_m = 1$. Consequently, it is necessary to consider the vernier effects in the calculation of back EMF of the model with the ratio of three slots/four magnet poles even though the voltage from common PM flux is still dominant. Among the models in Table 2, two models with $p_m = 5$ of $n_{aux} = 2$ and $p_m = 8$ of $n_{aux} = 3$ have higher voltage from modulation flux than that from conventional PM flux, resulting in substantially higher net back EMF than other ones. In particular, the model with $p_m = 8$ for $n_{aux} = 3$ is almost 2.5 times the back EMF of the model with $p_m = 1$ at $n_{aux} = 1$.

Table 3. Flux densities and induced voltages of a conductor.

Aux. Pole Numbers n	PM Pairs p_m	$\hat{B}_{conv}$ (T)	$\hat{B}_{ver}$ (T)	$\hat{e}_{a.conv}$ (V/m)	$\hat{e}_{a.ver}$ (V/m)	$\hat{e}_a$ (V/m)
1	1	0.268	0.086	0.350	0.056	0.406
	2				0.225	0.575
2	1	0.293	0.069	0.384	0.018	0.402
	2				0.045	0.429
	4				0.182	0.565
	5				0.454	0.837
3	1	0.315	0.055	0.412	0.009	0.421
	2				0.021	0.433
	4				0.058	0.470
	5				0.090	0.502
	7				0.253	0.665
	8				0.991	0.991

From the results of Table 3, it can be summarized that the EMFs from modulation flux as well as conventional PM flux increases with increase of n_{aux}. The model with G_r less than 2 has negligible vernier effects which are those with $p_m = 1$ of $n_{aux} = 1$, $p_m = 1$ and 2 of $n_{aux} = 2$, and $p_m = 1, 2, 4,$ and 5 of $n_{aux} = 3$ while others show meaningful vernier effects in the back EMF. For convenient comparison, the back EMF results in Table 3 are plotted in Figure 4.
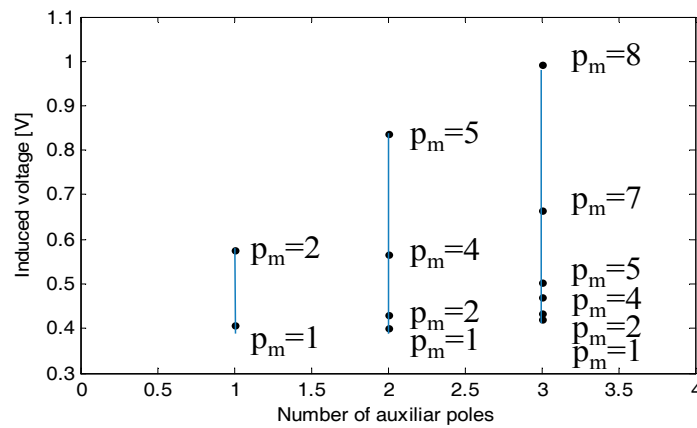
Figure 4. Induced voltages of a conductor of vernier machines.

Using the back EMF $\hat{e}_a$ of a single conductor in Table 3 and Figure 4, the back EMF in phase winding of each model can be easily calculated with (14) considering the winding factor due to the slot angle of $\pm 2/3\pi$ which will be compared with FE simulation results in the next section.

$$\widehat{E_b} = 2\sin\frac{2\pi}{3}N_{Ph}\hat{e}_a l_{stk} \tag{14}$$

*4.2. Models for Finite Element Analysis and Simulation Results*

Among the models in Table 3, five models in total are chosen for FE-analysis, and their detailed specifications are same as provided in Table 2. Two of them are the machines with $p_m = 1$ and 2 of $n_{aux} = 1$ which are chosen to confirm the vernier effects of the one with $p_m = 2$ since they have been commonly considered as conventional machines. In other words, their back EMFs should be same according to the classical machine theory, but will be different according to the results in Table 3. The other three models with $p_m = 5$ of $n_{aux} = 2$, and $p_m = 7$ and 8 of $n_{aux} = 3$ are chosen to verify the substantial back EMF boost effects. The stators of analysis models with $n_{aux} = 1$, 2, and 3 are shown in Figure 5, respectively where the slot open ratio of each model is 0.5. In addition, the thickness of the back yoke is determined considering flux per pole, so it is thinner as n_{aux} increases, which partially compensates the reduced slot area of the model with high n_{aux}.
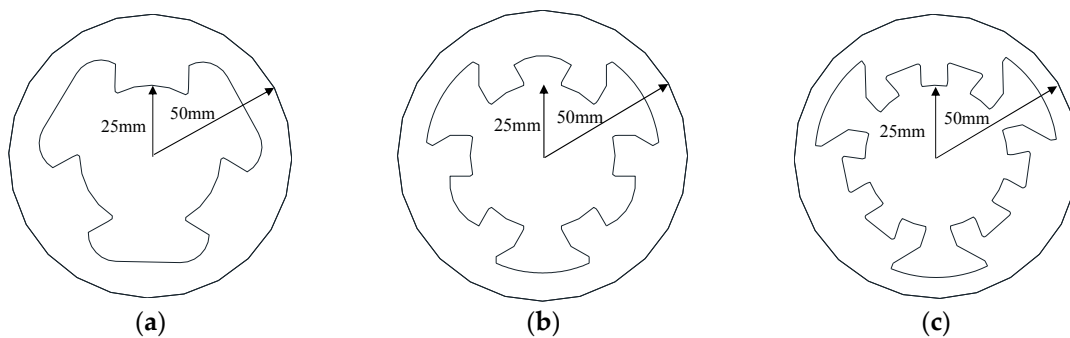
Figure 5. Stators with different auxiliary poles n_{aux} for FE simulations. (**a**) $n_{aux} = 1$; (**b**) $n_{aux} = 2$; (**c**) $n_{aux} = 3$.

For the analysis models with the stators in Figure 5 and the rotors having different p_m, the flux density and equipotential lines are solved with FEM and presented in Figure 6. It describes that the flux density of core and teeth is around 0.4~0.7 T, so there is no concern about saturation effects.
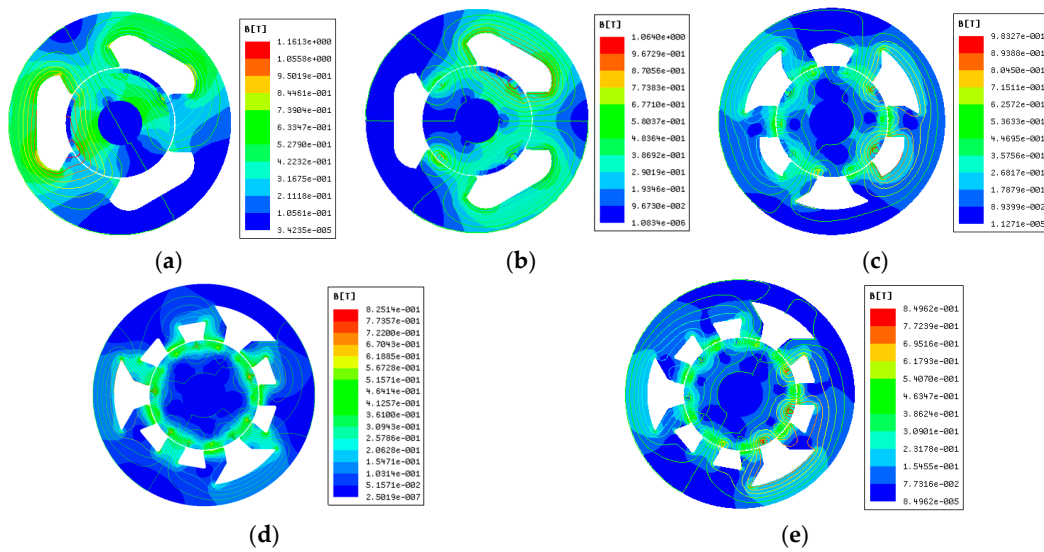
Figure 6. Flux density and equipotential lines of vernier motors for FE simulations. (**a**) $p_m = 1$ ($n_{aux} = 1$); (**b**) $p_m = 2$ ($n_{aux} = 1$); (**c**) $p_m = 5$ ($n_{aux} = 2$); (**d**) $p_m = 7$ ($n_{aux} = 3$); (**e**) $p_m = 8$ ($n_{aux} = 3$).

Under the established simulations conditions, the no-load back EMF of the analysis models at 500rpm are analyzed and the back EMF waveforms are plotted in Figure 7a. It shows that the model with $p_m = 8$ develops the highest back EMF, the next is the model with $p_m = 5$, and the last is the model with $p_m = 1$. Especially, the model with $p_m = 1$ has apparently less back EMF than the model with $p_m = 2$, clearly demonstrating the existence of vernier effects on the back EMF. The magnitudes of the first harmonics of the back EMF waveforms in Figure 7a are obtained by discrete Fourier expansion and compared with the back EMFs analytically calculated from (14) in Figure 7b. It shows that both results are in good accordance whose difference is less than 5%. Consequently, it can be said that every model found by using the proposed method includes vernier effects, even though the effects of first one ($p_m = 1$) with $G_r = 1/2$ are very negligible.
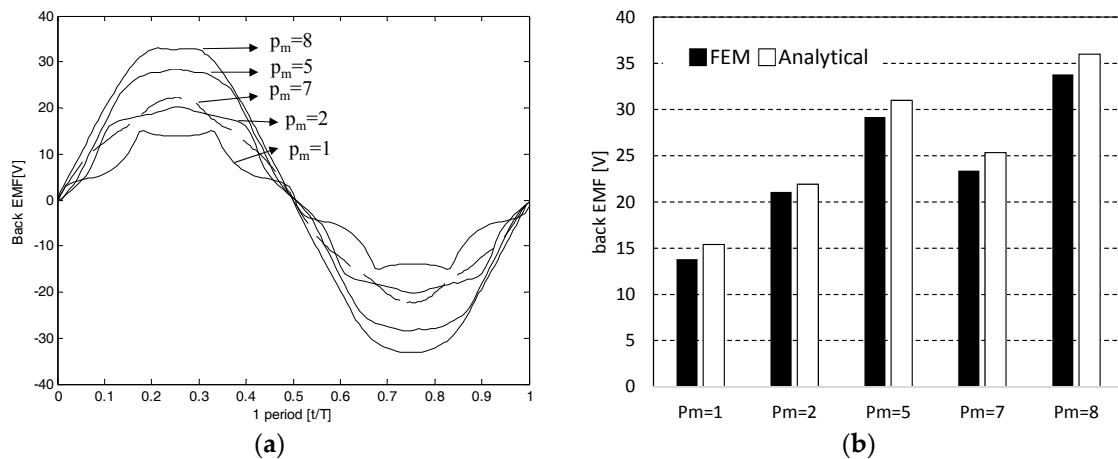
Figure 7. Comparison of Back EMF results. (**a**) Waveforms (FEM); (**b**) Magnitudes (FEM and analytical).

In addition, the characteristics of torque are calculated for the analysis models. FE-simulations are carried out with the phase current 2A (RMS) in phase with the back EMF, and the simulation results are depicted in Figure 8. It shows that the model with $p_m = 8$ of $n_{aux} = 3$ is about 2.5 times torque of the model with $p_m = 1$ of $n_{aux} = 1$, and overall characteristics coincide well with the back EMF results, which supports validity of the proposed assertion and effectively describes the advantage of vernier

machines with higher power density. It is also can be seen that the torque ripple characteristics are getting better with the increasing number of PMs.
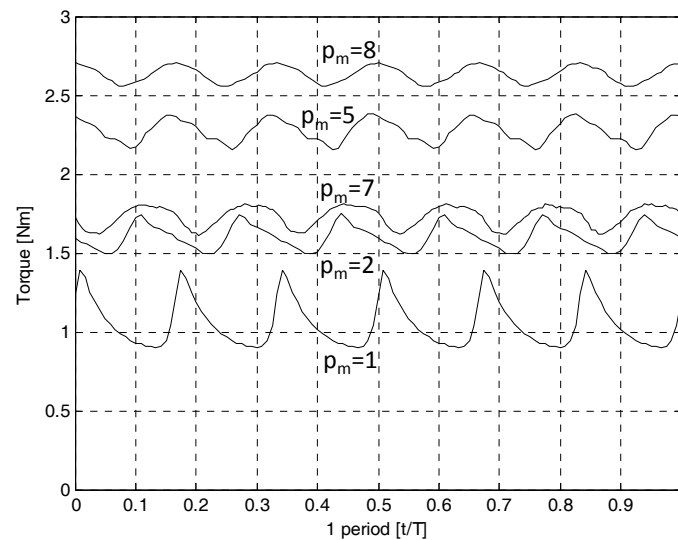

Figure 8. Torque characteristics of vernier motors (with 2A phase current).

5. Conclusions

In this study, to improve the theoretical uncertainty and restrictions in case that the previous design rule is applied to the machines with slot-concentrated windings, the necessary condition for effective utilization of vernier effects, $Q_{fmp} > p_m$, is firstly obtained, and then under the condition, the new criteria for slot–pole combinations were proposed for the most popular case of slot angle of $\pm 2/3\pi$ in the expression of well-organized form. It should be noted that the winding pole pairs, p_w of the FSPM machine is not necessary in the proposed criteria. Using the proposed criteria, every structure having vernier effects was found for a base FSCW PM machine with three stator slots and various auxiliary poles n_{aux}.

The investigation of the obtained FSCW-PM vernier machines are summarized as follows. First, in the obtained structures, many others are included which couldn't be found with the previous rules, which shows the versatility of the proposed criteria. Notably, it is shown that the PM machines with the slot/pole ratios of 3/2 and 3/4 are also included which have been considered as general ones without vernier effects. In addition, the model with $p_m = 7$ of $n_{aux} = 3$ is newly found and has quite big vernier effects which is hardly found by the previous design rule.

Using the obtained slot–pole combinations, practical FSCW-PM machines are designed with the same electric and magnetic loadings. The analytical calculations and FE analysis for the back EMF of the models are performed, and both results are in good accordance, indicating the usefulness of the air gap specific permeance functions expressed in terms of machine geometries. From the calculation results, it was proven that the obtained models from the proposed method have the vernier effect as expected, and the effects are dependent on the slot pole combinations. As expected, the model with three slots/four PM poles has higher back EMF than that with three slots/two PM poles due to higher gear ratio G_r. Therefore, it is necessary to consider the vernier effects in the accurate expression of performance characteristics such as the back EMF of those machines. The torque characteristics obtained through FE simulations presents good agreement with back EMF results, describing that the vernier motors have much higher power density than conventional PM machines. Finally, it can be said that the proposed method can be used in search for more candidates of PM vernier machines, and helps to make decisions about the best slot–pole combination in various conditions.

Conflicts of Interest: The authors declare no conflict of interest.

References

1. Li, D.; Qu, R.; Li, J.; Xiao, L.; Wu, L.; Xu, W. Analysis of Torque Capability and Quality in Vernier Permanent-Magnet Machines. *IEEE Trans. Ind. Appl.* **2016**, *52*, 125–135. [CrossRef]
2. Kim, B.; Lipo, T.A. Operation and Design Principles of a PM Vernier Motor. *IEEE Trans. Ind. Appl.* **2014**, *46*, 3656–3663. [CrossRef]
3. Kim, B.; Lipo, T.A. Analysis of a PM Vernier Motor with Spoke Structure. *IEEE Trans. Ind. Appl.* **2016**, *52*, 217–225. [CrossRef]
4. Li, D.; Qu, R.; Lipo, T.A. High-Power-Factor Vernier Permanent-Magnet Machines. *IEEE Trans. Ind. Appl.* **2014**, *46*, 3664–3674. [CrossRef]
5. Kim, B.; Lipo, T.A. Design of a Surface PM Vernier Motor for a Practical Variable Speed Application. In Proceedings of the IEEE Energy Conversion Congress and Exposition (ECCE), Montreal, QC, Canada, 20–24 September 2015; pp. 776–783.
6. Xu, L.; Liu, G.; Zhao, W.; Ji, J.; Zhou, H.; Zhao, W.; Jiang, T. Quantitative Comparison of Integral and Fractional Slot Permanent Magnet Vernier Motors. *IEEE Trans. Energy Convers.* **2015**, *30*, 1483–1495. [CrossRef]
7. Zou, T.; Qu, R.; Li, D.; Jiang, D. Synthesis of Fractional-Slot Vernier Permanent Magnet Machines. In Proceedings of the International Conference on Electrical Machines (ICEM), Lausanne, Switzerland, 4–7 September 2016; pp. 911–917.
8. Jian, L.; Xu, G.; Mi, C.; Chau, K.; Chan, C. Analytical Method for Magnetic Field Calculation in a Low-speed Permanent-magnet Harmonic Machine. *IEEE Trans. Energy Convers.* **2011**, *26*, 862–870. [CrossRef]
9. Li, J.; Chau, K.; Jiang, J.; Liu, C.; Li, W. A New Efficient Permanent-magnet Vernier Machine for Wind Power Generation. *IEEE Trans. Magn.* **2010**, *46*, 1475–1478. [CrossRef]
10. Okada, K.; Niguchi, N.; Hirata, K. Analysis of a Vernier Motor with Concentrated Windings. *IEEE Trans. Magn.* **2013**, *49*, 2241–2244. [CrossRef]
11. Heller, B.; Hamata, V. *Harmonic Field Effects in Induction Machines*; Elsevier Scientific Publishing Co.: Amsterdam, The Netherlands, 1977; pp. 54–67.
12. Bianchi, N.; Bolognani, S.; Pré, M.; Grezzani, G. Design Considerations for Fractional-Slot Winding Configurations of Synchronous Machines. *IEEE Trans. Ind. Appl.* **2006**, *42*, 997–1006. [CrossRef]
13. Hendershot, J.R., Jr.; Miller, T.J.E. *Design of Brushless Permanent-Magnet Motors*; Clarendon: Oxford, UK, 1994; pp. 4:10–4:15.
14. Pyrhonen, J.; Jokinen, T.; Hrabovcova, V. *Design of Rotating Electrical Machines*; Wiley: Hoboken, NJ, USA, 2008; pp. 92–100.